Ocean Modelling 183 (2023) 102200

Contents lists available at ScienceDirect

Ocean Modelling

journal homepage: www.elsevier.com/locate/ocemod

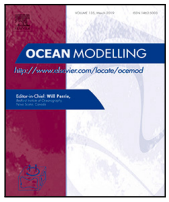

Ensemble-based data assimilation of significant wave height from Sofar Spotters and satellite altimeters with a global operational wave model

Isabel A. Houghton *, Stephen G. Penny, Christie Hegermiller, Moriah Cesaretti, Camille Teicheira, Pieter B. Smit

Sofar Ocean, Pier 28, San Francisco, 94105, CA, USA

ARTICLE INFO

Dataset link: http://dx.doi.org/10.5061/dryad.b5mkkwhh9

Keywords:
Wave data assimilation
LETKF
Ensemble data assimilation
Sofar Spotter wave buoys

ABSTRACT

An ensemble-based method for wave data assimilation is implemented using significant wave height observations from the globally distributed network of Sofar Spotter buoys and satellite altimeters. The Local Ensemble Transform Kalman Filter (LETKF) method generates skillful analysis fields resulting in reduced forecast errors out to 2.5 days when used as initial conditions in a cycled wave data assimilation system. The LETKF method provides more physically realistic model state updates that better reflect the underlying sea state dynamics and uncertainty compared to methods such as optimal interpolation. Skill assessment far from any included observations and inspection of specific storm events highlight the advantages of LETKF over an optimal interpolation method for data assimilation. This advancement has immediate value in improving predictions of the sea state and, more broadly, enabling future coupled data assimilation and utilization of global surface observations across domains (atmosphere-wave-ocean).

1. Introduction

Data assimilation (DA) with global operational wave models has lagged advances in other domains despite the value of accurate wave state representation for both wave forecasting itself and coupled Earth system forecasting more generally. In this work, we demonstrate the effective implementation of an ensemble-based wave data assimilation method that is a fundamental and, as of yet, not broadly implemented building block to a modern coupled Earth system forecasting framework.

The continuous development of Earth system modeling frameworks for weather forecasting has enabled remarkable increases in predictive ability with major social and economic consequences (Kull et al., 2021). This forecast skill is often attributed to a combination of improved model accuracy and observation utilization (Kalnay, 2002). Thus, effectively leveraging observations in Earth system modeling (i.e., data assimilation) is critically important to improving forecast skill. In the wave domain, the massive expansion of in situ observations provided by the Sofar Spotter network furthers the impact of DA developments.

Over the past 30 years, the production of ensemble forecasts has become a standard activity at operational weather prediction centers (Buizza, 2019; Kalnay, 2019). While operational centers generally produce *atmospheric* ensemble forecasts using some kind of ensemble-based or hybrid ensemble-variational DA method (Kleist and Ide, 2015; Rabier et al., 2000; Clayton et al., 2013), operational *wave* forecasts have generally been produced using either basic DA methods (Janssen et al., 2005) or no DA at all (NCEP, 2022).

Here, we aim to advance the DA capabilities for operational wave forecasting to catch up with the state of the art in atmospheric and oceanic prediction. While wave forecast skill improvement from DA has been demonstrated (Lionello et al., 1992; Aouf et al., 2006; Sanchez-Arcilla et al., 2021; Smit et al., 2021; Houghton et al., 2022) and approaches using Kalman filters (Emmanouil et al., 2012) or ensemble covariances (Sannasiraj et al., 2006) have been successfully demonstrated, this work presents the robust implementation of advanced ensemble DA methods in the wave domain at a global scale and in an operational capacity. The ensemble DA approach is advantageous because it can better leverage the uncertainty information provided by atmospheric ensemble forecasts driving the wave forecasts. Further, with the increasing trend toward the use of coupled forecasting systems (Janssen et al., 2005; Mehra and Yang, 2020), the proposed LETKF wave DA approach serves as a precursor to initializing a coupled numerical weather prediction system that properly leverages information about cross-domain atmosphere-wave-ocean dynamics.

With the advent of a globally distributed, high-density hourly in situ observing network provided by Sofar Spotter wave buoys (Houghton et al., 2021) in addition to satellite altimetry, impacts to forecast skill from wave observations at a global scale have become feasible. Smit et al. (2021) demonstrated a first implementation of assimilation of

* Corresponding author.
E-mail address: isabel.houghton@sofarocean.com (I.A. Houghton).

https://doi.org/10.1016/j.ocemod.2023.102200
Received 30 January 2023; Received in revised form 6 April 2023; Accepted 10 April 2023
Available online 21 April 2023

the global Spotter wave buoy network using a simple optimal interpolation scheme to assimilate measurements of significant wave height. Houghton et al. (2022) extended that work with an augmented optimal interpolation approach utilizing the spectral information provided by the Spotter buoys (frequency spectrum and Fourier coefficients of the directional spectrum). Both schemes provided forecast skill improvements for significant wave height out to three days, with additional benefits to peak and mean frequency and direction statistics for the spectral method.

Despite clear value demonstrated by the assimilation of measurements derived from this global network, there remain several challenges for skillful wave forecasting enabled by data assimilation, namely,

- Efficient determination of the forecast error covariances,
- Proper update to the model state (wave spectra) given observations of diverse integral parameters, and
- Capacity to correct the wind forcing field based on observed errors in the wind sea.

In this work, we describe the implementation of an ensemble-based data assimilation system using the Sofar Spotter network and satellite altimeters with the Local Ensemble Transform Kalman Filter (LETKF) (Hunt et al., 2007). LETKF combines the state-dependent background error derived from an ensemble forecast with the observations (and their corresponding uncertainties) to produce an analysis ensemble. In contrast to optimal interpolation (OI), where a fixed forecast error covariance length scale and structure (e.g., Gaussian) is prescribed, LETKF produces updates in the posterior analysis reflective of underlying uncertainty.

Further, LETKF allows for the simultaneous assimilation of a variety of observation types, as long as an observation operator to transform the model estimate to the observation space exists and observational uncertainty can be properly parameterized. In the case of a wave model, significant wave height observations from buoys and satellites can be assimilated and an analysis model spectra can be calculated without any assumptions regarding the relationship between an analysis significant wave height and the corresponding spectrum. In contrast, in optimal interpolation frameworks, the analysis is provided in the observation space. Therefore, for significant wave height or other directional wave buoy observations, some assumptions are required to return to the model space of a two dimensional frequency-direction spectrum (e.g., Lionello et al. (1992), Voorrips et al. (1997) and Houghton et al. (2022)). This functionality of LETKF becomes particularly valuable with the combination of the wave spectra observations from the Spotter network and significant wave height from satellite altimeters — both uniquely valuable observations that can be simultaneously assimilated in an LETKF framework. Finally, the LETKF implementation is ideally suited for a coupled model infrastructure (Sluka et al., 2016; Penny et al., 2019), enabling correction of the atmospheric domain based on errors observed in the wave domain - a promising avenue for longer lead time improvements in the wave forecast and overall improvements in a coupled atmosphere-wave system.

Motivated by the myriad of advantages afforded by an ensemble-based assimilation framework, we demonstrate how the utilization of significant wave height observations from approximately 600 free-drifting Spotter buoys and 3 satellite platforms (Jason-3, SARAL, and Sentinel-6A) leads to improvements in RMSD of forecasted ocean surface wave heights that can persist out to 60 h or more, and improvements in biases can persist beyond that. We also show specific examples demonstrating the value of state-dependent forecast error covariance information, and impacts on predicting swell arrival time. To understand the unique aspects of LETKF as a method, an OI assimilation and forecasting framework is also implemented for comparative purposes. Sections 2.1–2.2 describe the ensemble set up and processing of observations. Sections 2.3–2.6 describe the LETKF method and implementation choices, cycled analysis set up and forecast skill assessment. Section 3 discusses results, followed by conclusions and future work in Section 4.

2. Methods

In general, the data assimilation methods are evaluated in a cycled DA framework. For both the deterministic (OI) and ensemble (LETKF) methods, every hour, a one hour wave forecast (or ensemble of forecasts) is produced and used as the background in the assimilation step. The respective update method is then applied (OI or LETKF) and the analysis fields are then used as the initial conditions to the subsequent hour forecast.

2.1. Wave model ensemble

The WAVEWATCH3 (WW3) model (Tolman et al., 2019) is used to produce a 29-member ensemble wave forecast. Each member is identically implemented with 0.5° horizontal resolution over the global ocean and forced by an ensemble of near-surface (U_{10}) wind fields from the European Centre for Medium-Range Weather Forecasts (ECMWF) Ensemble forecast system. Members 1–29 of the ECMWF atmospheric ensemble are used (member 0 is the control run and not used), with each wind ensemble member consistently mapped to the same wave ensemble member at every model forecast step. A single deterministic sea ice area fraction forecast from the ECMWF High Resolution (HRES) forecast system is used for every wave ensemble member. Wave–current interactions, including relative wind effects, are included using HYCOM surface currents (Wallcraft, 2003). The WW3 model spectra are discretized with 36 equally-spaced direction bins and 36 logarithmically-spaced frequency bins. See Smit et al. (2021) for full WW3 model configuration details. Atmospheric forcing is updated every 6 h, as available from ECMWF.

In pre-processing, the zonal and meridional components of each ECMWF wind ensemble member are shifted such that the square of the ensemble mean (proportional to the wind stress driving wave growth) matches the square of the HRES wind in order to reduce biases in the wave ensemble. Further, the wind input source term calibration factor (β_{max}) (Ardhuin et al., 2010) in the ensemble wave model is reduced to 1.42 from the deterministic model value of 1.48.

2.2. Observation processing methods

Significant wave height (H_s) observations are used from the global Sofar Spotter network and the altimeters on three satellites. The Spotter buoy is an approximately 42 cm-diameter directional wave buoy that provides, in near real-time, hourly observations of the directional wave spectrum, sea surface temperature, barometric pressure, sound level pressure, surface drift and inferred wind (Houghton et al., 2021). Bulk wave parameters are calculated on board from the directional spectrum. In this work, only the significant wave height is utilized in the data assimilation framework. Prior to each analysis cycle, the Spotter data is aggregated and linearly interpolated onto the hour to align with the hourly WW3 model analysis times. Significant wave height observations below 0.2 m, above 25 m, or with an hourly difference larger than 5 m are removed. Approximately 600 Spotter observations are available each hour throughout the study.

Satellite altimeter observations of significant wave height are utilized from the Jason-3, SARAL, and Sentinel-6A platforms (SENTINEL-6, 2021; NASA/JPL, 2013; Desai, 2016). These data are ingested prior to an analysis cycle in an operational framework (i.e., near real-time), therefore only approximately 50% of the total number of altimeter observations are available at the time of analysis. Altimeter observations are binned to the nearest hour and the mean within a 0.5 degree latitude-longitude bin is stored (i.e. forming “super-obs” (Abdalla, 2014)). Latitude-longitude bins with a standard deviation of observations greater than 0.2 m are removed. Observations below 0.5 m, above 12 m and north or south of 60° are removed to avoid ice regions. A land mask is derived from the WW3 model grid and dilated by 6 grid cells to remove any observations within approximately

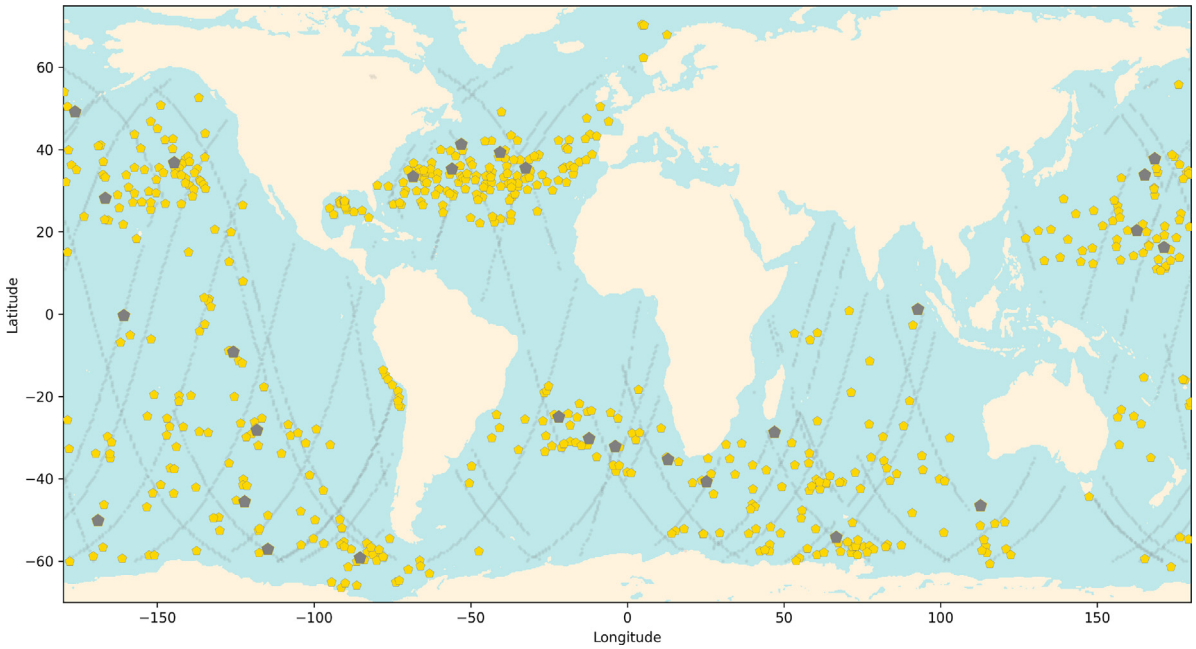

Fig. 1. An overview map of the global observations on October 25, 2022. This includes 605 total Sofar Spotters (gold pentagons) reporting hourly data and a cumulative 24 h of satellite altimeter tracks (gray dots) available within our operational time constraints. 28 Spotters were excluded (gray pentagons) from the data assimilation and used for forecast skill assessment.

300 km of land. Lastly, the altimeter observations are thinned by down-sampling to every other bin to reduce redundant information.

Processed observations are calculated and stored independently of the assimilation experiments such that all re-analyses use identical observation data. Fig. 1 illustrates Spotter buoy locations at the beginning of the study along with 24 h of aggregated altimeter tracks.

2.3. Local Ensemble Transform Kalman Filter (LETKF)

We implement LETKF following Hunt et al. (2007). Each background wave ensemble member (i.e. N grid points × 36 frequency bins × 36 direction bins) is used to construct the columns of the matrix $\hat{\mathbf{X}}^b$. The ensemble perturbations are then derived as $\mathbf{X}^b = \hat{\mathbf{X}}^b - \mathbf{1}^T\bar{\mathbf{x}}^b$, where $\bar{\mathbf{x}}^b$ is the background ensemble mean. LETKF balances the prior forecast error covariance estimated as $\mathbf{P}^b = \frac{1}{k-1}\mathbf{X}^b\mathbf{X}^{bT}$ with the observation error covariance, $\mathbf{R}$, to produce an optimal estimate of the posterior analysis ensemble $\mathbf{X}^a$. The effective Kalman gain, $\mathbf{K}$, of the LETKF algorithm can be formulated compactly as

$$\mathbf{K} = \mathbf{X}^b\left[\frac{k-1}{\rho}\mathbf{I} + \left(\mathbf{Y}^b\right)^T\mathbf{R}^{-1}\left(\mathbf{Y}^b\right)\right]^{-1}\left(\mathbf{Y}^b\right)^T\mathbf{R}^{-1}. \tag{1}$$

The matrix $\mathbf{Y}^b = H(\mathbf{X}^b)$ corresponds to the ensemble of model estimates transformed to the observation space by the observation operator H, which allows these states to be compared directly to observations. The integer k is the number of ensemble members and the scalar ρ is a multiplicative inflation parameter, used to maintain spread in the ensemble. The observation error covariance matrix $\mathbf{R}$ describes the expected observation errors on the diagonal and the covariances between observation errors on the off-diagonal.

Following the implementation by Hunt et al. (2007), the Kalman gain in Eq. (1) is a function of the model analysis error covariance, which is given in the ensemble perturbation subspace as,

$$\tilde{\mathbf{P}}^a = \left[\frac{k-1}{\rho}\mathbf{I} + \left(\mathbf{Y}^b\right)^T\mathbf{R}^{-1}\left(\mathbf{Y}^b\right)\right]^{-1}. \tag{2}$$

The updated state estimate is then provided by

$$\bar{\mathbf{x}}^a = \bar{\mathbf{x}}^b + \mathbf{K}\left(\mathbf{y}^o - H(\bar{\mathbf{x}}^b)\right), \tag{3}$$

where $\mathbf{y}^o$ is the set of observations and $\bar{\mathbf{x}}^a$ and $\bar{\mathbf{x}}^b$ correspond to the ensemble mean of the analysis and background, respectively. The updated set of ensemble perturbations in the original model space is provided by the transform operation,

$$\mathbf{X}^a = \mathbf{X}^b\left[(k-1)\tilde{\mathbf{P}}^a\right]^{\frac{1}{2}}. \tag{4}$$

The final analysis ensemble is then given as,

$$\hat{\mathbf{X}}^a = \mathbf{X}^a + \mathbf{1}^T\bar{\mathbf{x}}^a, \tag{5}$$

with negative values in the analysis set to zero.

Thus, every hour the observations available are optimally incorporated to generate an analysis ensemble with a mean representing the best estimate of the true state and a standard deviation representative of model uncertainty. In practice, the analysis wave spectrum at a gridpoint is the weighted sum of the ensemble members, with the weights determined by the LETKF method (see Hunt et al. (2007) for computationally efficient implementation details).

2.3.1. Implementation specifics

A multiplicative inflation of 5% ($\rho = 1.05$) is used to maintain ensemble spread over cycled analysis steps. Every analysis update decreases the spread of the ensemble members, however, the multiplicative inflation and the strong response to wind forcing avoids any collapse of the wave ensemble members over time. A test of relaxation to prior spread (Whitaker and Hamill, 2012) as an alternative to multiplicative inflation yielded similar results. Multiplicative inflation is thus chosen for simplicity.

An ensemble size of 29 is used to balance computational cost with achieving sufficient forecast ensemble spread. An inspection of observed and modeled significant wave height indicated that the ensemble spread sufficiently spans observation values. That said, a larger ensemble could more reliably represent the true state and remove spurious correlations in space.

Due to the use of finite ensemble size, possible spurious correlations in space could degrade the analysis. To mitigate this issue, a limit on the physical distance of an observation used in the analysis is imposed - i.e. localization. The localization is applied with a weighting function that decays with distance (d), a maximum cutoff distance for relevant

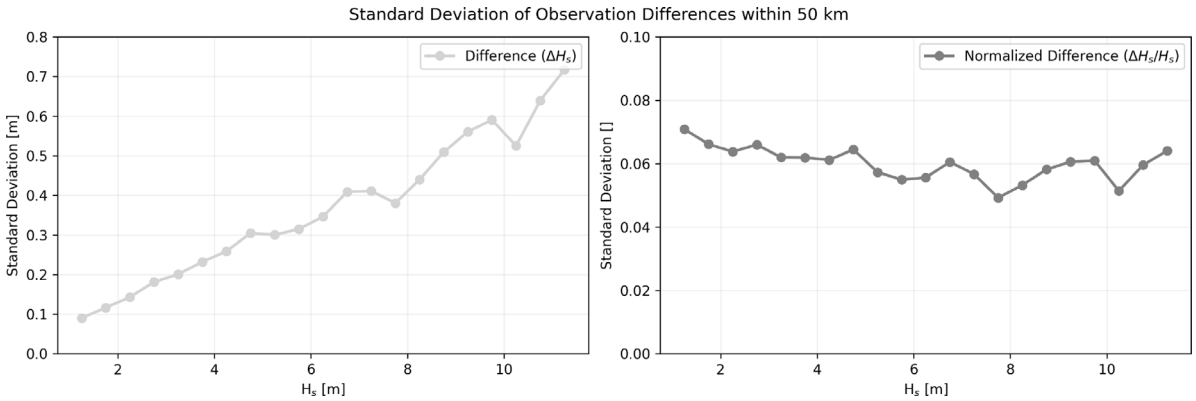

Fig. 2. Pairs of Spotters within 50 km were aggregated from the drifting network historical archive. The differences between the reported wave heights for each pair were used to estimate the expected standard deviation of observation errors parameterized in the assimilation. A strong dependence on wave state was observed (left). Normalizing the difference by the average wave height observed yielded a relatively constant value of expected errors used in the data assimilation (right).

observations and an upper limit on number of observations included. A horizontal length-scale, σ_h, of 800 km is used to determine the observation weight following,

$$w(d) = e^{-0.5(\frac{d}{\sigma_h})^2}. \tag{6}$$

A maximum cutoff distance (influenced by Gaspari and Cohn (1999)) is then derived from the horizontal length scale of

$$d_{max} = 2\sqrt{10/3}\ \sigma_h \approx 2900 \text{ km}. \tag{7}$$

A maximum of 5 Spotter observations and 30 altimeter observations are used for analysis at any given grid point. For a grid point with greater than the maximum number of observations, the most proximate observations are used.

To derive the model estimates in the observation space, $H(\mathbf{X}^b)$, the model spectrum is bi-linearly interpolated to the observation location and then the significant wave height, H_s, is calculated following

$$H_s = 4\sqrt{\int\int E(f,\theta)\mathrm{d}f\,\mathrm{d}\theta}, \tag{8}$$

where $E(f,\theta)$ is the model state, the variance density spectrum in frequency (f) and direction (θ).

2.3.2. Observation error covariances

Data assimilation relies on balancing uncertainty in the model with uncertainty in the observations to provide a best estimate of the true state. As a result, a reliable estimate of uncertainty in observations relative to the model is critical, spanning observational noise and representativeness errors (Janjić et al., 2018). To that end, a co-location study was carried out to estimate uncertainty in Spotter observations. Over approximately a one year period, all Spotter observations collected within 50 km were co-located, and the differences between proximate observations were aggregated. A maximum separation distance of 50 km was chosen to incorporate representativeness error of the 0.5° model grid along with observational noise and yielded approximately 93,000 pairs. A consistent difference in observed wave heights as a function of wave height itself is observed (Fig. 2). Specifically, higher sea states resulted in larger differences between co-located observations. This proportional scaling of uncertainty is consistent with uncertainty associated with integrals over observed spectra (Young, 1986) - rather than instrument GPS error. As a result, a relative observation error standard deviation is chosen. Within the assimilation framework, the observation error is estimated unique to each observation as 6.5% of the observation value itself for Spotters. Off-diagonal observation error covariances are assumed to be zero for significant wave height, simplifying the **R** matrix to be diagonal and increasing computational speed of the LETKF algorithm. A moderately higher uncertainty is attributed to the satellite altimeter of 10% motivated by observed noise in the satellite observations (Abdalla, 2014).

2.4. Wave model analyses

2.4.1. LETKF

Each ensemble member is initialized with the same model state from the free-running (non-assimilative) deterministic 0.5° model. A one hour forecast is carried out for each of the ensemble members to produce a background ensemble, $\hat{\mathbf{X}}^b$. The analysis step is then carried out using ensemble members 1–29. The analysis ensemble mean is then calculated and stored as the zeroth ensemble member. Ensemble member 0 is then driven by the deterministic (ECMWF HRES) winds, while the rest of the ensemble members are driven by their respective ensemble wind member. This architecture is chosen to propagate forward a "best estimate" of the analysis state, assuming the deterministic winds are more skillful than any individual wind ensemble member.

Spin-up of the wave ensemble is assessed with the global average standard deviation of the significant wave heights in the ensemble as a function of time and the distribution of departures ($\mathbf{y}^o - H(\hat{\mathbf{X}}^b)$). The model spread represented by the standard deviation of H_s and the mean of the departures are expected to stabilize for a spun-up cycled system, and appear to do so after approximately two days, or 48 analysis cycles.

2.4.2. Optimal interpolation

To assess the unique impacts of the LETKF assimilation technique given an equivalent set of observations, a comparative cycled analysis was also run using an optimal interpolation (H_s OI) scheme as outlined in Smit et al. (2021). A constant observation standard deviation of error of 0.3 m and a model error covariance scale of 0.3 m with homogeneous, isotropic structure was prescribed with a correlation length-scale of 300 km.

2.5. Wave model forecasts

Every six hours, the deterministic wind and sea ice fields provided by ECMWF HRES are used to drive three-day forecasts initialized by the wave model analyses. Three different experiments are presented here — LETKF, Optimal Interpolation (OI), and free-running (No DA). For LETKF, the best estimate ensemble mean assigned to the zeroth ensemble member is used as the initial condition to the four-day forecast. For OI, simply the analysis field at the forecast initialization time is used. For No DA, the 6-hour forecast from the previous forecast initialization is used. The wave model is implemented identically as for the ensemble above, except utilizing ECMWF HRES winds and the corresponding β_{max} of 1.48. Therefore, differences in forecast skill should be attributable to the initialization alone. Forecasts were initialized after a spin-up of 48 analysis cycles and run from October 12, 2022 to November 2, 2022.

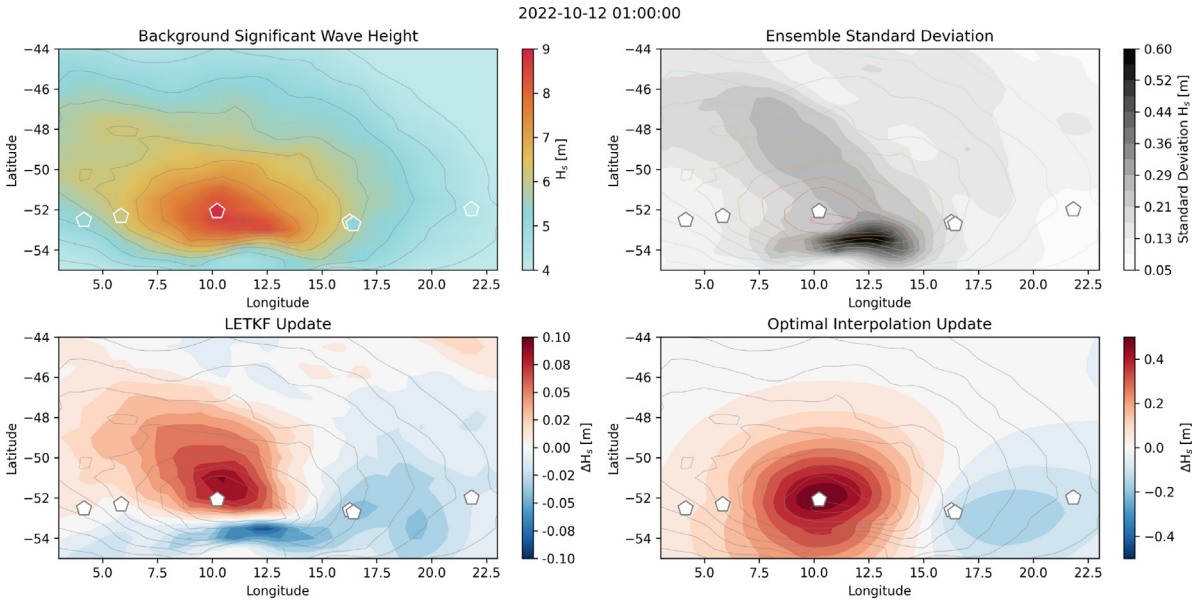

Fig. 3. An example of model increments for LETKF and OI assimilation methods. Upper left: A large storm with waves upwards of 9 m was predicted in the Southern Ocean around October 12, 2022. Contours indicate the magnitude of significant wave height and are overlaid on all subplots to visualize storm location. Spotter locations are indicated by pentagonal markers, colored by observed significant wave height. Upper right: Model spread is illustrated with the standard deviation of the significant wave height among the 29 ensemble members. Lower left: The model increment (analysis — background) from the LETKF method. The wave heights are increased in the upper half of the storm and reduced in the lower half. Lower right: The model increment from the OI method. To note, the magnitudes of the updates are larger for the optimal interpolation framework, an indication that the assimilation is not well-balanced with the model state.

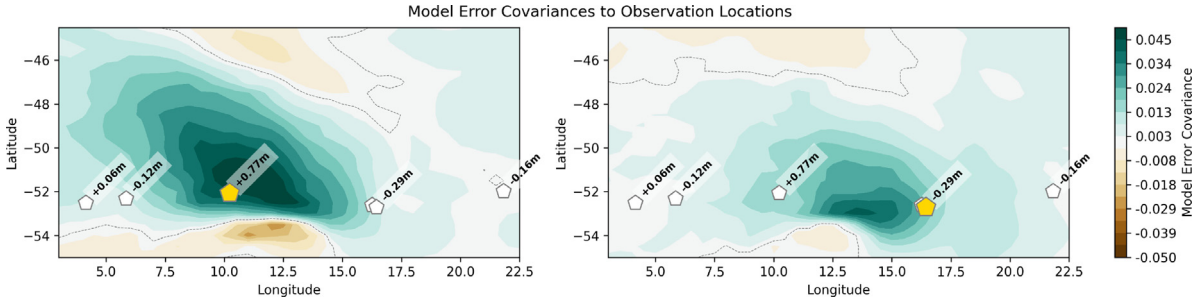

Fig. 4. An example of the model error covariances derived from the significant wave height fields of the ensemble for two locations with a Spotter buoy (yellow pentagon) present. The gray contour line indicates an error covariance of zero to the indicated observation location, the cross over from a positive correlation to a negative correlation of model errors. Departures (observation — model) are shown for each observation.

2.6. Forecast skill assessment

Forecast skill is assessed by bi-linearly interpolating model significant wave height to excluded (un-assimilated) Spotter and altimeter observations. Bias (mean error) and root-mean-square error (RMSE) are evaluated for significant wave height as a function of forecast lead time. In addition to the globally aggregated statistics, specific events are inspected to illustrate the differences between the two assimilation techniques and the non-assimilative forecast.

3. Results

The LETKF data assimilation runs in the cloud on 28 cores with up to 60 GB of memory in approximately 0.4 h per hourly analysis-forecast cycle (2.5 h between the 6-hourly forecast initialization), and is therefore feasible to operationalize, such as for the currently operational Sofar wave forecast used for ship routing optimization.

3.1. Analysis increment

The differences between the OI and LETKF techniques are well-illustrated by inspection of the model analysis increment ($\bar{\mathbf{x}}_a - \bar{\mathbf{x}}_b$). Fig. 3 illustrates the increment in terms of significant wave height, an integral property of the sea state that is physically interpretable. For a large storm in the Southern Ocean with H_s exceeding 9 m, the LETKF model ensemble exhibits a large spread among members, or model uncertainty, in the southern region of the storm, illustrated with the standard deviation of H_s (Fig. 3, upper right). Inspection of the difference in the wave heights calculated from the model ensemble analysis and background indicate a unique spatial structure to the update. This update is reflective of both the model uncertainty and the structure of the model error covariances (Fig. 4). Specifically, the Spotter observation in the center of the storm reported wave heights higher than the model background. At the same time, there exist large, positive error covariances between the location of the observation and the northern portion of the storm and a negative error covariance in the southern flank of the storm (orange-brown shading in Fig. 4). As a result, in the LETKF analysis, significant wave height is adjusted higher near to and north of the Spotter observation, and adjusted lower to the south. This inverse update (lowering waves to the south, despite a positive departure) in essence shifts the storm further north, enabled by the model error covariances calculated from the ensemble. In contrast, the optimal interpolation update (Fig. 3, lower right) is a Gaussian-looking fit to the observations present, with the largest update applied

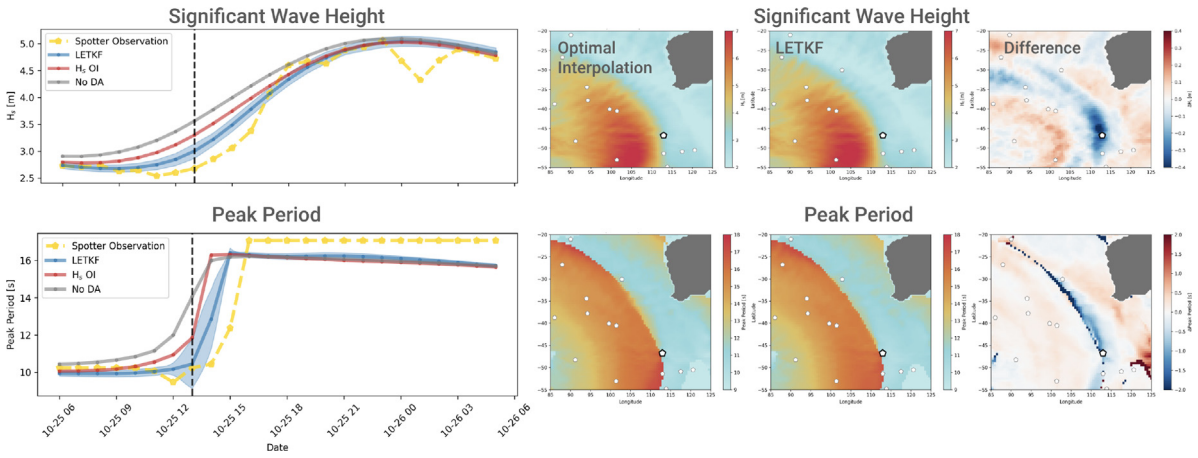

Fig. 5. An inspection of a storm event to the southwest of Australia. Left: Time series from a forecast initialized on October 24 18:00 UTC show significant wave height and peak period at an excluded Spotter buoy. The Spotter observations (yellow) indicate a later arrival of the high wave heights compared to No DA (gray), H_s OI (red), and LETKF (blue). LETKF most closely predicts the arrival of the long period, fastest waves associated with the storm, indicated by the jump in peak period. The LETKF time series envelope (shaded blue) indicates the standard deviation of the analysis ensemble at the observation time, an additional feature of LETKF not otherwise available. Right: Spatial maps of significant wave height and peak period at the 19-hour lead time illustrate the spatial structure of differences between the two cycled data assimilation frameworks (OI and LETKF). LETKF results in a decrease of the eastern edge of the storm and increase to the north, in better agreement with observations.

exactly at the observation location, regardless of underlying sea state structure. As a result, rather than shifting the storm in space, the overall energy of the storm is inflated within the covariance length-scale of the observation. Further, the magnitude of the model increments varies between LETKF and OI (10 cm versus 40 cm, respectively). Owing to the cycled nature of the assimilation systems and relatively constant locations of the Spotter observations hour-to-hour, each analysis step should only be a small nudge toward the "true state" that is applied sequentially and should be in balance with the wave model and overlying wind forcing. The much larger increments associated with OI likely indicate updates that are out of balance with the model state and external forcing and as a result are destroyed with each model forecast step, only to be reintroduced with each subsequent analysis.

3.2. Forecast time series

Ultimately, the analysis update is sought to provide an accurate initial condition for forecasting. Inspection of discrete events highlights the performance of LETKF versus OI and No DA for forecast initialization. During a high wave event around October 25, 2022 to the southwest of Australia, the 1 day forecast provided by LETKF indicates improved performance for prediction of storm arrival. Fig. 5 displays time series at an excluded Spotter location and corresponds to forecasts initialized on October 24, 2022 18:00 UTC. At approximately October 25 13:00 UTC, a distinct jump in peak period is present in the observation, indicating the arrival of the swell generated by the storm. The No DA forecast predicts the swell arrival approximately 3 h too early, OI approximately 2 h early and LETKF approximately 1 h early. The predictions of significant wave height are offset similarly. Inspecting the spatial fields at the 19-hour lead time (Fig. 5, right), the LETKF forecast compared to the OI forecast indicates a distinct reduction in peak period and significant wave height at the leading edge of the storm, resulting in the delayed storm arrival in better agreement with the Spotter observation.

3.3. Aggregated forecast skill

In all forecasts, root-mean-square error of H_s increases as a function of forecast lead time (Fig. 6). For the forecasts initialized by LETKF and OI analyses, the global RMSE at short lead times (0–12 h) is reduced by up to 24% compared to the non-assimilative forecast. At longer lead times, all forecasts converge, as is expected with identical forcing and model configuration. When compared to satellite altimeter observations of significant wave height, LETKF narrowly outperforms OI at all lead times. When comparing to excluded Spotter observations, OI outperforms LETKF at the shorter lead times (0 and 6 h), and otherwise follows similar trends as the altimeter comparison for longer lead times. While the skill is evaluated at excluded Spotters only, the free-drifting Spotters tend to cluster and are very rarely present entirely independent of neighboring Spotters (see Fig. 1). As a result, the skill at excluded Spotters is more reflective of the short term impact of pulling toward observations near utilized Spotters, whereas the skill at excluded altimeters is likely more representative of updates to the entire ocean domain, including further afield of included observations.

4. Discussion and conclusion

For the first time, an ensemble-based data assimilation method for wave forecasting is implemented using observations from the global Sofar Spotter buoy network and satellite altimeters. This implementation yields global wave forecast skill improvement over a non-assimilative forecasting framework, with additional improvements over optimal interpolation when inspecting individual events.

By utilizing the ensemble to estimate the model error covariances, LETKF provides an analysis increment reflective of the underlying sea state and model uncertainty, in contrast to an OI method. This novel capability enables physically meaningful updates to the model background, such as shifting a storm in space or maintaining sharp gradients that would otherwise be smoothed by OI. Minor shifts in storm location or swell arrival can be of particular value for applications such as ship routing, where certain vessels are highly sensitive to wave period. For coastal applications, variations in swell arrival time on the order of a couple hours can result in differences in coastal impacts due to combinations with tide and surge phasing. Consequently, incremental improvements in representation and forecasting of the sea state is of particular value.

While LETKF appears particularly skillful for discrete events, it remains comparable to OI in an aggregate sense. OI is a simple, yet effective, tool when evaluated near where the updates are occurring and in terms of RMSE of significant wave height - a metric that does not necessarily capture more complex features that are also of importance (e.g. small-scale structure, arrival timing of large events). That said, the superior performance of LETKF when compared to altimeter observations indicates the ability of LETKF to provide skillful updates far from observations by leveraging understanding of the model error covariances in a way that OI fundamentally cannot do. Further optimization of the LETKF implementation (e.g., tuning background ensemble

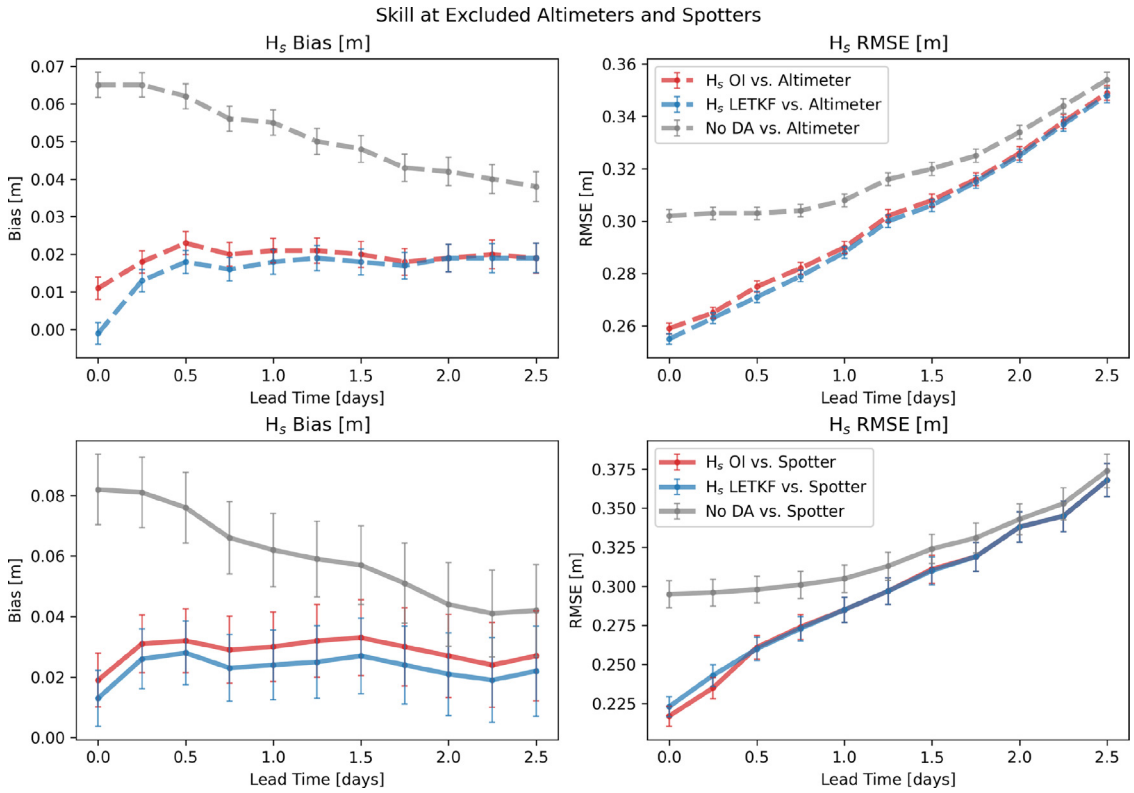

Fig. 6. Forecast skill for significant wave height. Bias (left) and root-mean-square error (RMSE) (right) are calculated as a function of forecast lead time. Skill is evaluated at excluded altimeter observations (top) and excluded Spotters (bottom) for the No DA (gray), H_s OI (red) and LETKF (blue) forecasting frameworks. Uncertainty estimates in the bias and RMSE are represented by the error bars following Jensen (2017).

model skill, observation error covariances, localization, multiplicative inflation) may serve to reduce forecast errors further. Regardless, the primary objective of the implementation presented herein is the robust ensemble-based approach to enable more advanced implementations in a coupled Earth system model framework.

An efficient and skillful LETKF implementation for wave forecasting is critical for future development of coupled Earth system modeling frameworks. Specifically, with access to an ensemble, the errors in the wave domain can then correct the atmospheric domain. By extending the observations provided by the comprehensive global Spotter network to atmospheric corrections, the potential for both unique atmospheric forecast improvements *and* wave forecast skill improvements at longer lead times (where errors are nearly entirely determined by errors in the overlying winds) becomes feasible.

Further, LETKF is particularly well-suited to handle diverse sets of observations – such as wave spectra and significant wave heights – simultaneously. Previously, Houghton et al. (2022) utilized the rich and unique dataset of observations of directional wave spectra available from the Sofar Spotters. These observations were assimilated in an optimal interpolation framework to achieve marked improvements in forecast skill of wave period and direction, which are also critical variables in wave forecast accuracy. This first LETKF implementation described here focuses solely on significant wave height for the development of a robust underlying system. However, future work will be the augmentation of observational variables to include the frequency-dependent information on total energy and directional distribution. LETKF is ideally suited for handling the diverse types of observations from altimeters (H_s alone) and Spotters, and a frequency-localized update of the model state is expected to allow for skillful improvement of both the sea and swell components more independently. Further, Spotter provides observations at the air–sea interface beyond the sea state, including barometric pressure and sea surface temperature. Combining the vast network of Spotter observations and data provided by satellite altimeters in a coupled model framework with the data assimilation strategy demonstrated here could lead to additional forecast improvements across global oceans.

CRediT authorship contribution statement

Isabel A. Houghton: Conceptualization, Methodology, Formal analysis, Investigation, Writing – original draft. **Stephen G. Penny:** Conceptualization, Methodology, Writing – review. **Christie Hegermiller:** Conceptualization, Methodology, Writing – review. **Moriah Cesaretti:** Software. **Camille Teicheira:** Software. **Pieter B. Smit:** Conceptualization, Supervision, Project administration.

Declaration of competing interest

The authors declare the following financial interests/personal relationships which may be considered as potential competing interests: All authors reports financial support was provided by Office of Naval Research. All authors reports a relationship with Sofar Ocean Technologies, Inc that includes: employment.

Data availability

Data and software specific to this study can be found at doi:http://dx.doi.org/10.5061/dryad.b5mkkwhh9.

Acknowledgments

S.G. Penny acknowledges support from the Office of Naval Research (ONR), United States of America grants N00014-19-1-2522 and N00014-20-1-2580, National Aeronautics and Space Administration (NASA) grant 80NSSC21K1363 and National Oceanic and Atmospheric Administration (NOAA) grant NA22OAR4590510.

All authors acknowledge support from the Office of Naval Research (ONR) grant N00014-22-1-2394.

References

Abdalla, S., 2014. Active techniques for wind and wave observations: Radar altimeter. In: Proceedings of the Seminar on Use of Satellite Observations in Numerical Weather Prediction, Reading, UK. pp. 8–12.

Aouf, L., Lefèvre, J.-M., Hauser, D., 2006. Assimilation of directional wave spectra in the wave model WAM: An impact study from synthetic observations in preparation for the SWIMSAT satellite mission. J. Atmos. Ocean. Technol. 23 (3), 448–463. http://dx.doi.org/10.1175/JTECH1861.1, URL: https://journals.ametsoc.org/view/journals/atot/23/3/jtech1861_1.xml.

Ardhuin, F., Rogers, E., Babanin, A.V., Filipot, J.-F., Magne, R., Roland, A., Van Der Westhuysen, A., Queffeulou, P., Lefevre, J.-M., Aouf, L., et al., 2010. Semiempirical dissipation source functions for ocean waves. Part I: Definition, calibration, and validation. J. Phys. Oceanogr. 40 (9), 1917–1941.

Buizza, R., 2019. Introduction to the special issue on "25 years of ensemble forecasting". Q. J. R. Meteorol. Soc. 145 (S1), http://dx.doi.org/10.1002/qj.3370.

Clayton, A.M., Lorenc, A.C., Barker, D.M., 2013. Operational implementation of a hybrid ensemble/4D-var global data assimilation system at the met office. Q. J. R. Meteorol. Soc. 139 (675), http://dx.doi.org/10.1002/qj.2054.

Desai, S., 2016. Jason-3 GPS based orbit and SSHA ogdr. http://dx.doi.org/10.5067/J3L2G-OGDRF, URL: https://podaac.jpl.nasa.gov/dataset/JASON_3_L2_OST_OGDR_GPS.

Emmanouil, G., Galanis, G., Kallos, G., 2012. Combination of statistical Kalman filters and data assimilation for improving ocean waves analysis and forecasting. http://dx.doi.org/10.1016/j.ocemod.2012.09.004.

Gaspari, G., Cohn, S.E., 1999. Construction of correlation functions in two and three dimensions. Q. J. R. Meteorol. Soc. 125 (554), 723–757.

Houghton, I.A., Hegermiller, C., Teicheira, C., Smit, P.B., 2022. Operational assimilation of spectral wave data from the sofar spotter network. Geophys. Res. Lett. 49 (15), e2022GL098973. http://dx.doi.org/10.1029/2022GL098973, URL: https://agupubs.onlinelibrary.wiley.com/doi/abs/10.1029/2022GL098973.

Houghton, I.A., Smit, P.B., Clark, D., Dunning, C., Fisher, A., Nidzieko, N.J., Chamberlain, P., Janssen, T.T., 2021. Performance statistics of a real-time Pacific ocean weather sensor network. J. Atmos. Ocean. Technol. 38 (5), 1047–1058. http://dx.doi.org/10.1175/JTECH-D-20-0187.1, URL: https://journals.ametsoc.org/view/journals/atot/aop/JTECH-D-20-0187.1/JTECH-D-20-0187.1.xml.

Hunt, B.R., Kostelich, E.J., Szunyogh, I., 2007. Efficient data assimilation for spatiotemporal chaos: A local ensemble transform Kalman filter. Physica D 230 (1), 112–126. http://dx.doi.org/10.1016/j.physd.2006.11.008, URL: https://www.sciencedirect.com/science/article/pii/S0167278906004647.

Janjić, T., Bormann, N., Bocquet, M., Carton, J.A., Cohn, S.E., Dance, S.L., Losa, S.N., Nichols, N.K., Potthast, R., Waller, J.A., et al., 2018. On the representation error in data assimilation. Q. J. R. Meteorol. Soc. 144 (713), 1257–1278.

Janssen, P., Bidlot, J.-R., Abdalla, S., Hersbach, H., 2005. Progress in Ocean Wave Forecasting at ECMWF. ECMWF Technical Memorandum.

Jensen, J., 2017. Which method is more accurate? or errors have error bars. http://dx.doi.org/10.7287/peerj.preprints.2693.

Kalnay, E., 2002. Atmospheric modeling, data assimilation and predictability. In: Atmospheric Modeling, Data Assimilation and Predictability. http://dx.doi.org/10.1017/CBO9780511802270.

Kalnay, E., 2019. Historical perspective: earlier ensembles and forecasting forecast skill. Q. J. R. Meteorol. Soc. 145 (S1), http://dx.doi.org/10.1002/qj.3595.

Kleist, D.T., Ide, K., 2015. An OSSE-based evaluation of hybrid variational-ensemble data assimilation for the NCEP GFS. Part I: System description and 3D-hybrid results. Mon. Weather Rev. 143 (2), http://dx.doi.org/10.1175/MWR-D-13-00351.1.

Kull, D., Riishojgaard, L.P., Eyre, J., Varley, R.A., 2021. The value of surface-based meteorological observation data. http://dx.doi.org/10.1596/35178.

Lionello, P., Gunther, H., Janssen, P.A., 1992. Assimilation of altimeter data in a global third-generation wave model. J. Geophys. Res. http://dx.doi.org/10.1029/92jc01055.

Mehra, A., Yang, F., 2020. Coupled model prototype5 (S2SP5). URL: https://vlab.noaa.gov/web/ufs-r2o/coupled-model-prototype5.

NASA/JPL, 2013. SARAL near-real-time value-added operational geophysical data record sea surface height anomaly. http://dx.doi.org/10.5067/AKASA-XOGD1, URL: https://podaac.jpl.nasa.gov/dataset/ALTIKA_SARAL_L2_OST_XOGDR.

NCEP, 2022. NWW3 implementations. URL: https://polar.ncep.noaa.gov/waves/implementations.shtml?.

Penny, S.G., Bach, E., Bhargava, K., Chang, C.-C., Da, C., Sun, L., Yoshida, T., 2019. Strongly coupled data assimilation in multiscale media: Experiments using a quasi-geostrophic coupled model. J. Adv. Modelling Earth Syst. 11 (6), 1803–1829. http://dx.doi.org/10.1029/2019MS001652, URL: https://agupubs.onlinelibrary.wiley.com/doi/abs/10.1029/2019MS001652.

Rabier, F., Järvinen, H., Klinker, E., Mahfouf, J.F., Simmons, A., 2000. The ECMWF operational implementation of four-dimensional variational assimilation. I: Experimental results with simplified physics. Q. J. R. Meteorol. Soc. 126 (564), http://dx.doi.org/10.1002/qj.49712656415.

Sanchez-Arcilla, A., Staneva, J., Cavaleri, L., Badger, M., Bidlot, J., Sorensen, J.T., Hansen, L.B., Martin, A., Saulter, A., Espino, M., Miglietta, M.M., Mestres, M., Bonaldo, D., Pezzutto, P., Schulz-Stellenfleth, J., Wiese, A., Larsen, X., Carniel, S., Bolaños, R., Abdalla, S., Tiesi, A., 2021. CMEMS-Based Coastal analyses: Conditioning, coupling and limits for applications. Front. Mar. Sci. 8, http://dx.doi.org/10.3389/fmars.2021.604741.

Sannasiraj, S.A., Babovic, V., Chan, E.S., 2006. Wave data assimilation using ensemble error covariances for operational wave forecast. Ocean Model. 14 (1–2), http://dx.doi.org/10.1016/j.ocemod.2006.04.001.

SENTINEL-6, 2021. Sentinel-6A MF/Jason-CS L2 P4 altimeter high resolution (HR) NRT ocean surface topography. http://dx.doi.org/10.5067/S6AP4-2HSNR, URL: https://podaac.jpl.nasa.gov/dataset/JASON_CS_S6A_L2_ALT_HR_STD_OST_NRT_F.

Sluka, T.C., Penny, S.G., Kalnay, E., Miyoshi, T., 2016. Assimilating atmospheric observations into the ocean using strongly coupled ensemble data assimilation. Geophys. Res. Lett. 43 (2), 752–759. http://dx.doi.org/10.1002/2015GL067238, URL: https://agupubs.onlinelibrary.wiley.com/doi/abs/10.1002/2015GL067238.

Smit, P.B., Houghton, I.A., Jordanova, K., Portwood, T., Shapiro, E., Clark, D., Sosa, M., Janssen, T.T., 2021. Assimilation of significant wave height from distributed ocean wave sensors. Ocean Model. 159, 101738. http://dx.doi.org/10.1016/J.OCEMOD.2020.101738.

Tolman, H., Abdolali, A., Accensi, M., Alves, J.-H., Ardhuin, F., Babanin, A., Barbariol, F., Benetazzo, A., Bidlot, J., Booij, N., Boutin, G., Bunney, C., Campbell, T., Chalikov, D., Chawla, A., Cheng, S., Collins, C., Filipot, J.-F., Flampouris, S., Liang, Z., 2019. User Manual and System Documentation of WAVEWATCH III (R) Version 6.07. Technical Report, URL: https://www.researchgate.net/publication/336069899_User_manual_and_system_documentation_of_WAVEWATCH_III_R_version_607.

Voorrips, A.C., Makin, V.K., Hasselmann, S., 1997. Assimilation of wave spectra from pitch-and-roll buoys in a north sea wave model. J. Geophys. Res. C: Oceans 102 (C3), 5829–5849. http://dx.doi.org/10.1029/96JC03242.

Wallcraft, A., 2003. Hybrid coordinate ocean model (HYCOM) user's guide. Manual.

Whitaker, J.S., Hamill, T.M., 2012. Evaluating methods to account for system errors in ensemble data assimilation. Mon. Weather Rev. 140 (9), 3078–3089. http://dx.doi.org/10.1175/MWR-D-11-00276.1, URL: https://journals.ametsoc.org/view/journals/mwre/140/9/mwr-d-11-00276.1.xml.

Young, I.R., 1986. Probability distribution of spectral integrals. J. Waterw. Port Coast. Ocean Eng. 112 (2), 338–341. http://dx.doi.org/10.1061/(ASCE)0733-950X(1986)112:2(338), URL: https://ascelibrary.org/doi/abs/10.1061/%28ASCE%290733-950X%281986%29112%3A2%28338%29.